31st Symposium on Naval Hydrodynamics
Monterey, California, 11-16 September 2016

Free Maneuvering Simulation of ONR Tumblehome Using Overset Grid Method in naoe-FOAM-SJTU Solver

Jianhua Wang, Weiwen Zhao, Decheng Wan
(State Key Laboratory of Ocean Engineering, School of Naval Architecture, Ocean and Civil Engineering, Shanghai Jiao Tong University, Collaborative Innovation Center for Advanced Ship and Deep-Sea Exploration, Shanghai, China)

ABSTRACT

In the past few decades, the growing capability of Computational Fluid Dynamics (CFD) has pushed the research in the field of ship hydrodynamics from simple to complex, covering the prediction of ship resistance, seakeeping, self-propulsion and maneuvering. However, the predictions of free maneuvering problems are especially difficult, mostly due to limitations of traditional meshing methodologies when handling with moving objects. In this paper, a series of numerical computations are carried out to study the free maneuvering characteristics of fully appended ONR Tumblehome ship model with twin rotating propellers and rudders. All the numerical simulations are carried out by our in-house solver naoe-FOAM-SJTU, which is developed on the open source platform OpenFOAM and mainly composed of a dynamic overset grid module and a full 6DoF motion module with a hierarchy of bodies.

The objective of this paper is to validate our CFD solver naoe-FOAM-SJTU in predicting free maneuvering problems. In the present work, CFD-based method coupling with dynamic overset grid approach is applied to investigate the free maneuvering tests, i.e. full 6DoF self-propulsion and turning circle tests. For the self-propulsion simulation, open water performance of the propeller and towed condition of bare hull will be computed beforehand. The simulation of the towed condition can give an approximate flow field of the self-propulsion and the flow field can be mapped as the initial state of the self-propulsion to reduce the large amount of calculation and avoid divergence at the beginning. Open water performance will give the hydrodynamic characteristics of the rotating propeller. Grid convergence study is applied in this condition to validate the numerical results and the computed results will also be compared with the experimental data. The full 6DoF self-propulsion is carried out by introducing a PI controller to update the rate of revolutions (RPS) of the propeller to achieve the target speed and a P controller for rudder to keep the ship going straight forward. The present numerical result for the RPS is underestimated by 1.7% compared with the experimental data, which indicates that the present approach is applicable for the full 6DoF self-propulsion simulation. As for the turning circle simulation, the fully appended ship hull is first going straight with the propeller RPS obtained by the previous self-propulsion calculation and then the ship rudder is gradually turned to the desired angle to start turning circle. Good agreement is achieved for the ship model trajectory. Furthermore, the detailed flow visualizations are also presented at several critical times during the transient phase for turning circle simulation with the aim to explain how the flow characteristics affect the hydrodynamic performance.

INTRODUCTION

Free maneuvering capabilities is a key standard to examine whether a ship has good maneuverability. Thus how to evaluate the maneuvering characteristics at the design stage is of great importance and the studies in this area have been extensively progressed. However, great challenges show up with the complexity of the flow field and interaction between hull, moving rudders and rotating propellers. When dealing with the fully appended ship, the vortical structures separated from the hull and appendages are even more complicated. For most other computations in ship hydrodynamics, the 6DoF motion is always simplified into 3 degrees of freedom, which is sufficient to handle ship resistance, seakeeping problems. But for free maneuvering, i.e. full 6DoF self-propulsion, turning circle, zigzag maneuver, the ship needs full 6DoF motion with moving rudders and rotating propellers in a free surface condition. All the above aspects increase the difficulty in the study of the free maneuvering problems.

Up to the present, the main method for predicting ship maneuverability still strongly relies on the experimental results, of which oscillatory motion tests and circular motion tests account for the main part. The capabilities of ship maneuvering can then be obtained by simplified mathematical models. Nowadays, the increasing demand of ship operating speed and high accuracy for ship maneuvering prediction with hull, rudder and propeller interaction has made it essential to develop free running model test in wave basins. Free running ship model with moving rudders and rotating propellers in wave basins requires more advanced measurement systems for both global and local flow variables. Furthermore, experimental uncertainty also plays an important role for the obtained data and it put forward high requirements for the experimental fluid dynamics (EFD) development. As stated above, experiment for free maneuvering test can be very expensive and there still has many challenges to accomplish this in traditional towing tank. Sanada et al. (2013), Elshiekh (2014) have done a series of free maneuvering experiment in IIHR wave basin for ONR Tumblehome in both calm water and regular waves and provide wide range of free maneuvering test data for CFD validation.

With the performance of computers boosting in the past few decades, tremendous advances have been made in the development of Computational Fluid Dynamics (CFD) on ship hydrodynamics. In addition, the dynamic overset grid method, including a hierarchy of bodies that enable computation of full 6DoF and moving components (rudders, propellers), makes it possible to directly compute self-propulsion and free maneuvering with rotating propellers and moving rudders. Nowadays, overset grid method has been applied to the computations of ship hydrodynamics, especially for the direct simulation of hull-propeller-rudder interaction. Carrica et al. (2012) uses RANS approach with dynamic overset grids to study the turn and zigzag maneuvers of a surface combatant. In his study, the propeller is modeled through a simple actuator disk/ body-force approach in which local velocity effects on the propellers are neglected. Numerical results are mostly within 10% compared to the experimental data. Broglia et al. (2015) takes the same approach for the turning simulation of a fully appended twin screw vessel using a finite volume method CFD solver. Further analysis for the distribution of forces and moments on the hull, appendages and rudders has been done to gain the dynamic behavior in turning tests. Shen et al. (2015) implements dynamic overset grid module to OpenFOAM and applied to the KCS self-propulsion and zigzag maneuvering simulation. Direct simulation of hull, propeller and rudder interaction is applied and the numerical results show that the overset grid method is applicable for the computations of ship hull, propeller and rudder interaction. Carrica et al. (2016) reported the direct simulation of zigzag maneuver for KCS in shallow water. Full discretized propeller model is used in this condition and grid uncertainty studies are also conducted with grids up to 71.3 million points. Direct simulated results show satisfactory agreements with the experimental results for most of the variables.

This paper presents our recent study progress in the numerical prediction of free maneuvering for fully appended ONR Tumblehome using overset grid method. The rotating propellers and moving rudders are directly discretized in this study. This paper is organized as follows: first is the numerical approach, which includes the introduction of naoe-FOAM-SJTU solver, dyamic overset grid technique, and feedback controller techniques for moving components; following this is the geometry model and grid distribution; then comes the simulation part, where towing condition, open water calculation, self-propulsion and turning circle simulation are presented systematically; in addition, grid convergence study is carried out for open water calculations. Finally, a conclusion of this study is drawn.

NUMERICAL APPROACH

naoe-FOAM-SJTU Solver

The CFD code naoe-FOAM-SJTU solves the Navier-Stokes equations for unsteady turbulent flows with VOF method capturing free surface around the complex geometry models. URANS equations are written as a mass conservation equation and a momentum conservation equation:

$$\nabla \cdot \boldsymbol{U} = 0 \tag{1}$$

$$\begin{aligned} \frac{\partial \rho \boldsymbol{U}}{\partial t} + \nabla \cdot \left[(\rho \boldsymbol{U} - \boldsymbol{U}_g)\boldsymbol{U} \right] &= -\nabla p_d - \boldsymbol{g} \cdot \boldsymbol{x} \nabla \rho \\ &+ \nabla \cdot (\mu_{eff} \nabla \boldsymbol{U}) + (\nabla \boldsymbol{U}) \cdot \nabla \mu_{eff} + f_\sigma \end{aligned} \tag{2}$$

where U is the fluid velocity field and U_g is the velocity of mesh points; $p_d = p - \rho \mathbf{g} \cdot \mathbf{x}$ is the dynamic pressure, obtained by subtracting the hydrostatic component from the total pressure; ρ is the mixture density of the two-phase fluid; $\boldsymbol{g}$ is the gravity acceleration; $\mu_{eff} = \rho(\nu + \nu_t)$ is the effective dynamic viscosity, in which ν and ν_t are the kinematic viscosity and kinematic eddy viscosity respectively, the latter one is obtained by the two-equation shear stress transport turbulence model ($SST\ k-\omega$, Menter, 2009); f_σ is a source term due to surface tension.

VOF method with bounded compression technique is applied to capture free surface and the transport equation is expressed as:

$$\frac{\partial \alpha}{\partial t} + \nabla \cdot \left[\left(\boldsymbol{U} - \boldsymbol{U}_g \right) \alpha \right] + \nabla \cdot \left[\boldsymbol{U}_r \left(1 - \alpha \right) \alpha \right] = 0 \tag{3}$$

where α is volume of fraction, 0 and 1 represent that the cell is filled with air and water respectively and $0<\alpha<1$ stands for the interface between two-phase fluid. $\boldsymbol{U}_r$ in Eqn. (3) is the velocity field used to compress the interface and it only takes effect on the free surface due to the term $(1-\alpha)\alpha$.

The framework of naoe-FOAM-SJTU solver and its main features are only briefly presented here; more details can be referred to Shen et al. (2014, 2015a, 2015b), Cao et al. (2014, 2015), and Wang et al. (2015a, 2015b). The solver is developed on the open source platform OpenFOAM and is mainly composed of a velocity inlet wave-making module, a full 6DoF module with a hierarchy of bodies and a mooring system module. The solver has the ability of handling varies problems in naval architecture and ocean engineering, i.e. large motion response for platforms in ocean waves; ship resistance, seakeeping prediction; ship self-propulsion and free maneuvering with moving rudders and rotating propellers.

The URANS equations and VOF transport equation are discretized by the finite volume method (FVM), and for the discretized URANS equations, the merged PISO-SIMPLE (PIMPLE) algorithm is applied to solve the coupled equations for velocity and pressure field. The Semi-Implicit Method for Pressure-Linked Equations (SIMPLE) algorithm allows to couple the Navier-Stokes equations with an iterative procedure and the Pressure Implicit Splitting Operator (PISO) algorithm enables the PIMPLE algorithm to do the pressure-velocity correction. More detailed description for the SIMPLE and PISO algorithm can be found in Ferziger and Peric (1999) and Issa (1986). In addition, several built-in numerical schemes in OpenFOAM are used in solving the partial differential equations (PDE). The convection terms are discretized by a second-order TVD limited linear scheme, and the diffusion terms are approximated by a second-order central difference scheme. Van Leer scheme (Van Leer, 1979) is applied for VOF equation discretization and for the steady problems, such as towing condition, Euler scheme is applied for temporal discretization, while for the transient problems, the temporal term is discretized by a second-order backward scheme.

Overset Grid Technique

The overset grid module is the key point for direct simulating the full coupled hull, propeller and rudder system. So a brief introduction of the utilization of overset grid module in naoe-FOAM-SJTU solver is presented. Overset grid comprises of two or more blocks of overlapping structured or unstructured grids. By using dynamic overset grid techniques, the overlapping grids can move independently without constraints. To achieve this, the cells in the computational domain are classified into several types, i.e. fringe, hole, donor etc. The information of these is contained in the domain connectivity information (DCI) file. In our present solver, Suggar++ (Noack et al., 2009) is utilized to generate the domain connectivity information (DCI) for the overset grid interpolation. To combine OpenFOAM with Suggar++, a communication, which is responsible for DCI exchange between OpenFOAM and Suggar++, has been implemented using the Message passing interface (MPI) library (Shen et al., 2015). Other features consist of a full 6DoF motion module with a hierarchy moving components and several modifications for sparse matrix solvers and MULES solver to excluded non-active cells.

With the dynamic overset grid capability, the full 6DoF motion solver allows the ship hull as well as the moving components to move simultaneously. Two coordinate systems are used to solve the 6DoF equations. One is the inertial system (earth-fixed system) and the other is non-inertial system (ship-fixed system). The inertial system can be fixed to earth or move at a constant speed with respect to the ship (here we only apply the horizontal motion for the moving of inertial system). The non-inertial system is fixed to the ship and can translate or rotate according to the ship motions. Details of the 6DoF module with overset grid module implementation can be found in Shen et al., (2015). In our present study, the complex geometry is decomposed into several overlapping grids, and can be used to handle complex motion problems, especially for the numerical simulation of self-propulsion and free maneuvering.

Feedback Controllers for Moving Components

Ship self-propulsion and free maneuvering requires the operation on the control of moving components (rudders and propellers). In order to achieve the simulations mentioned above, controllers for the moving components are utilized into the solver to accomplish the simulation.

For full 6DoF self-propulsion simulation, the propellers need to provide the thrust for the ship to advance and the rudders need to move to achieve the target heading. A proportional-integral (PI) controller is applied to adjust the rotational rate of the propeller to achieve the target ship speed. The instantaneous RPS of the propeller is calculated as:

$$n = Pe + I\int_0^t edt \tag{4}$$

where P and I are proportional and integral constants respectively, and e is the error between target ship speed and instantaneous speed:

$$e = U_t - U_i \tag{5}$$

The PI controller is activated at the beginning of the calculation and updates the rate of revolutions of the propeller (RPS) at the end of each time step. The rate of revolutions of the propeller *n* is adjusted to obtain force equilibrium in the longitudinal direction:

$$T = R_{T(SP)} \tag{6}$$

where T is the computed thrust, $R_{T(SP)}$ is the total resistance of the self-propulsion model in calm water.

Rudders are deflected with following proportional control equation:

$$\delta(t) = K_P\left(\psi(t) - \psi_C\right) \tag{7}$$

where $\delta(t)$ is rudder angle, $\psi(t)$ is yaw angle, $\psi_C = 0$ is target yaw angle, and proportional gain $K_P = 1.0$. Rudder angle update at the end of each time to achieve the target yaw angle.

For the turning circle simulation, the rate of revolutions of the propellers *n* is set to fixed value (obtained from the final convergence state of self-propulsion simulation) and the rudders first turn to the desired angle (here 35° to the starboard) at appropriate rudder rate $35^\circ/s$ and then the ship is under turning circle condition. The rudders turn back to initial state when the ship model needs to pull out.

GEOMETRY AND GRID DISTRIBUTION

Numerical simulations were carried out for the ONR Tumblehome model 5613, which is a preliminary design of a modern surface combatant fully appended with skeg and bilge keels. The model also has rudders, shafts and propellers with propeller shaft brackets. The geometry of ONR Tumblehome is shown in Figure 1, and the principle geometric characteristics are listed in Table **1**. The ship model is used as one of the benchmark cases in Tokyo 2015 CFD workshop in ship hydrodynamics. Extensive experiments were performed at IIHR basin for this ship model and the available experimental data can be used to validate our computational results.

Figure 1 Geometry of ONR Tumblehome

Table 1 Main particulars of ONR Tumblehome

Main particulars		Model scale	Full scale
Length of waterline	L_{WL} (m)	3.147	154.0
Maximum beam of waterline	B_{WL} (m)	0.384	18.78
Depth	D (m)	0.266	14.50
Draft	T (m)	0.112	5.494
Displacement	Δ (kg)	72.6	8.507e6
Wetted surface area (fully appended)	S_0 (m^2)	1.5	NA
Block coefficient (CB)	$\nabla/(L_{WL}B_{WL}T)$	0.535	0.535
LCB	LCB (*m*) aft of FP	1.625	NA
Vertical center of gravity (from keel)	KG (*m*)	0.156	NA
Metacentric height	GM (*m*)	0.0422	NA
Moment of inertia	K_{xx}/B_{WL}	0.444	0.444
Moment of inertia	K_{yy}/L_{WL}, K_{zz}/L_{WL}	0.246	0.25
Propeller diameter	D_P (m)	0.1066	NA
Propeller shaft angle (downward pos.)	ε (*deg.*)	5	NA
Propeller rotation direction (from stern)		inward	inward
Maximum rudder rate		35.0 deg./s	

For the self-propulsion and turning circle simulations, the computational domain is divided into six parts: one for the background grid, one for grid around ship hull, two for the grids around propeller in starboard side and port side, two parts for both side rudders. Six part grids have overlapping areas and the grid arrangement is shown in Figure 2.

The rudders and propellers are able to rotate with respect to the ship hull and provide the thrust forces and turning moments for the ship, respectively. For the self-propulsion simulation, the background domain extends to $-1.5L_{pp} < x < 5.0L_{pp}$, $-1.5L_{pp} < y < 1.5L_{pp}$, $-1.0L_{pp} < z < 0.5L_{pp}$, and the hull domain is much smaller with a range of $-0.15L_{pp} < x < 1.2L_{pp}$, $-0.13L_{pp} < y < 0.13L_{pp}$, $-0.2L_{pp} < z < 0.2L_{pp}$. But for the turning circle simulation, the background domain extends to $-1.0L_{pp} < x < 3.0L_{pp}$, $-1.0L_{pp} < y < 1.0L_{pp}$, $-1.0L_{pp} < z < 0.5L_{pp}$ in consideration of reducing the computing time.

All grids used in this paper are generated by *snappyHexMesh*, a mesh generation tool provided by OpenFOAM. The total grid number of the simulation is 6.81M and 6.36 M for self-propulsion and turning circle respectively. The detailed grid information in each part is shown in Table 2. Considering the grid quality in overlapping areas, several refinement boxes are applied to offer enough donor cells for interpolation. Grids in gaps between rudders and propellers should be taken good care of and grid size in overlapping areas should be approximately at the same size. Good grid quality at overlapping areas can resolve better flow information and reduce the computational time. The global and local mesh distribution around ship hull is shown in Figure 3 and Figure 4 respectively.

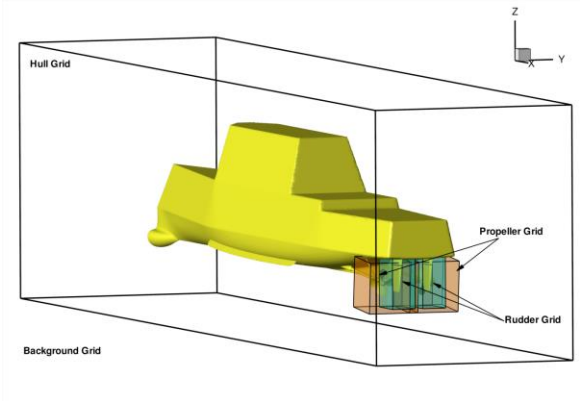

Figure 2 Grid arrangement around ship hull

Table 2 Grid distribution in each part

Grid	Total	Port	Starboard
Total*	6.81M	--	--
Background*	1.34M	--	--
Hull	2.61M	--	--
Propeller	2.28M	1.14M	1.14M
Rudder	0.58M	0.29M	0.29M

*The grid number here is just for the self-propulsion simulation, and the grid number of turning circle is 6.36M only with less grid number in background.

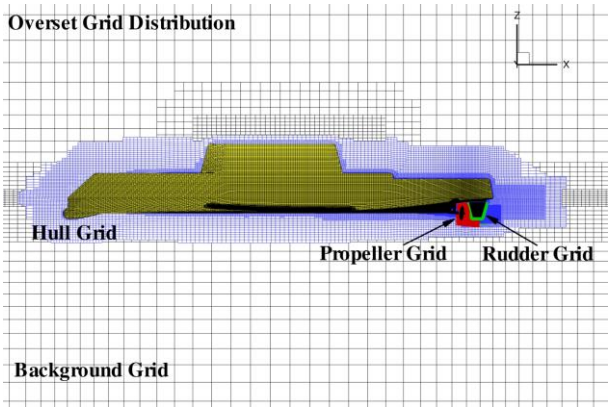

Figure 3 Global mesh distribution

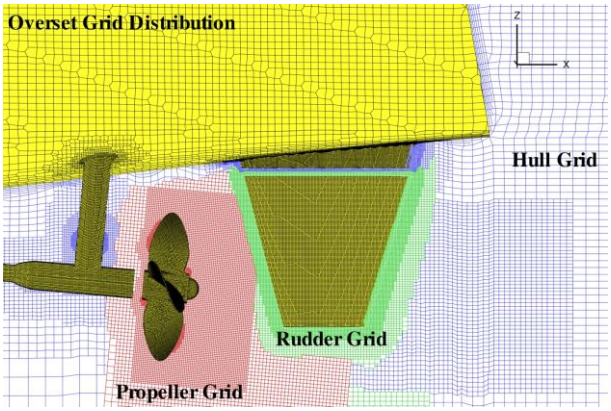

Figure 4 Local mesh distribution

SIMULATION PART I: SELF-PROPULSION

Open Water Calculation for Propeller

Before simulating full 6DoF self-propulsion, open water calculation for the propeller is carried out. Calculated open water curves will be compared with the experimental results performed at IIHR (available at Tokyo 2015 CFD Workshop). The comparison between the numerical results and experimental data can be used to validate the current dynamic overset grid approach in simulating rotating propellers.

In the present study, open water curves are obtained by the single-run procedure described in Xing et al. (2008). During the single-run calculation, the propeller is towed with a small acceleration to fulfil a wide range of advance velocities in one single-run. The

computational domain is divided into two parts, i.e. background grid and propeller grid. When doing the calculation, the propeller grid rotates with the rotating propeller while the background grid moves forward with the advancing velocity. The number of the unstructured grids is about 1.13M with 0.51M for propeller grid and 0.62M for background grid. The grid distribution around propeller is shown in Figure 5.

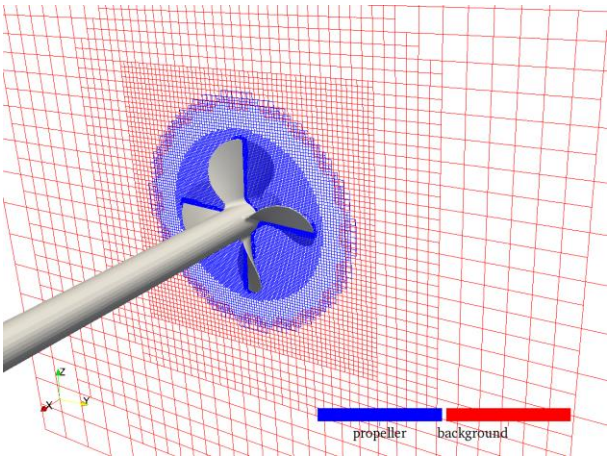

Figure 5 Grid distribution around propeller

During the procedure, the rate of resolution of propeller is set to fixed value and the advancing speed is chosen to achieve the desired advance coefficient J . Thrust coefficients K_T , torque coefficient K_Q and efficiency η_0 for each advance coefficient are obtained from the calculated thrust and torque. The propulsive coefficients mentioned above are defined as:

$$J = \frac{V_A}{nD} \tag{8}$$

$$K_T = \frac{T}{\rho n^2 D^4} \tag{9}$$

$$K_Q = \frac{Q}{\rho n^2 D^5} \tag{10}$$

$$\eta_0 = \frac{JK_T}{2\pi K_Q} \tag{11}$$

where T and Q are the propeller thrust and torque, D is the diameter of propeller, n is the RPS and V_A is the advancing speed. The rate of resolution of propeller is set to n=8.97 according to the experimental setup for self-propulsion. The experimental data for the open water characteristics are available at Tokyo 2015 CFD Workshop in ship hydrodynamics.

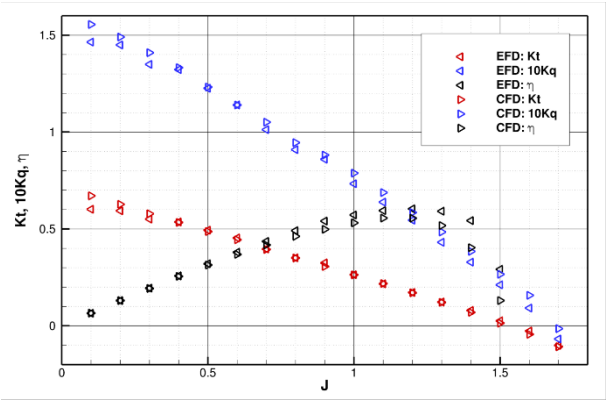

Figure 6 Open water curves of experiment (left triangle symbol) and single-run approach CFD results (right triangle symbol)

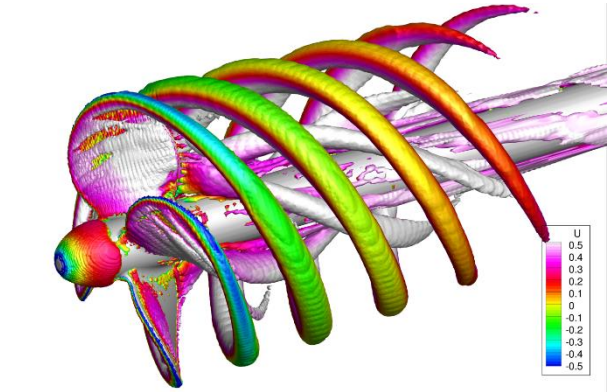

a) J=0.8

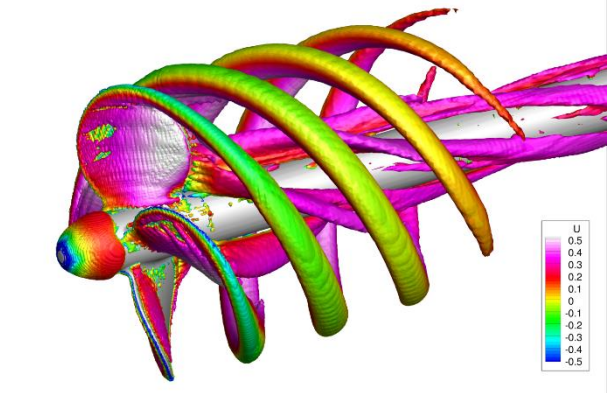

b) J=1.0

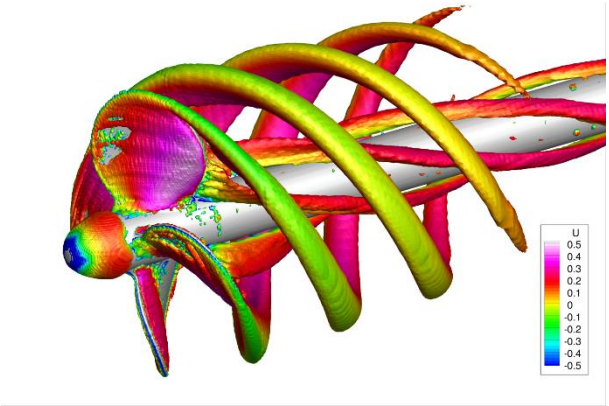

c) J=1.2

Figure 7 Isosurfaces of Q=200 at different advance coefficients colored by velocity magnitude.

The simulating results of the open water curves are shown in Figure 6. The propeller accelerates from J=0 to J=1.8 in 10 seconds. The predicted open water results have an overall agreement with the experimental data expect for $J > 1.3$, where the efficiency η_0 is underestimated. Figure 7 shows the vortical structures using isosurfaces of Q=200 and colored by the axial velocity. From the figure we can see that the tip vortices are resolved clearly, and as the advance coefficient increases the strength of the tip vortices decrease a lot. This is due to the fact that the angle of attack decreases when the advance coefficient becomes larger.

The hub vortices also show the same trend with the strength decreasing. Because of the rather coarse mesh and the RANS turbulence model, the shape of vortical structures are stable and no vortex-pairing effect is observed. In spite of the limitations of RANS model, the calculated coefficients K_T, K_Q and η_0 are well predicted by the present dynamic overset grid method coupled with the single-run approach.

The numerical computations for the open water characteristics are performed with 20 processors at the HPC cluster (IBM nx360M4, 2.8GHZ) in our research group. 19 processors are assigned to compute the flow information and 1 processor is given to SUGGAR++ processor to do the DCI computation. The time step is set to $\Delta t = 5 \times 10^{-4}$ s and the end time of the computation is 10s. The total computational time for the open water case is about 26h with grid number of 1.13M.

Towed Condition for Ship Hull

The towed condition is following the experimental setup, and the advancing speed is $U = 1.11 m/s$, with the Froude Number of $Fr = 0.20$. The simulation is carried out without appendages and moving components. Overset grid approach is also applied in this simulation, and the computational domain is separated into the hull grid and background grid shown in Figure 8. The total grid number is 1.87M, with 0.82M for hull grid and 1.05M for background grid. The boundary conditions are identical with zero velocity and zero gradient of pressure imposed on inlet and far-field boundaries. The outlet boundary applies a special velocity boundary called the *outletPhaseMeanVelocity*, which is a built-in scheme in OpenFOAM and this boundary condition adjust the velocity for the given phase to achieve the specified mean thus causing the phase-fraction to adjust according to the mass flow rate. The hull grid is embedded in the background grid that covers the computational domain and is used to impose the far-field boundary conditions.

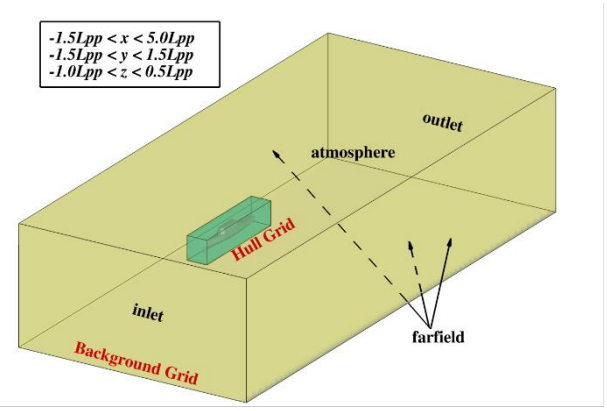

Figure 8 Computational domain for towing condition

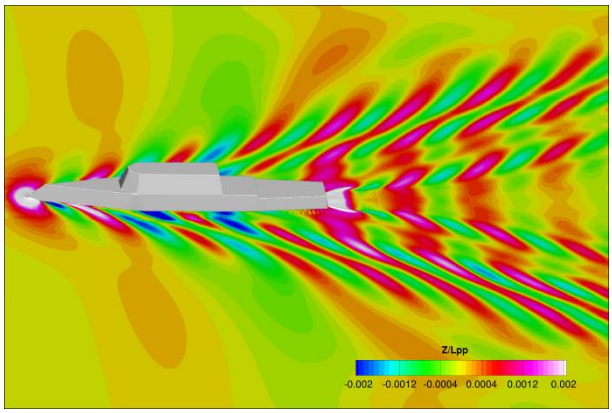

Figure 9 Wave pattern for bare hull

During the calculation, the ship model moves forward at the desired speed U_0 and the other 5 degrees of freedom are fixed. In this way, the calculated flow field can be used as an initial state for the self-propulsion state. This step can save a lot of computational time by starting the calculation with a developed flow field and boundary layer. Cook (2011) investigate the appendages effect on the total resistance for ONR Tumblehome model in

different Froude numbers, and the comparison between the present numerical results and the experimental data as well as CFD results by IIHR are listed in Table 3. The present results for the bare hull resistance show satisfactory agreement with the EFD data performed at INSEAN and the CFD results from IIHR. The calculated wave pattern is shown in Figure 9.

Table 3 Total resistance comparison with bare hull

F_r	IIHR EFD* fully appended	INSEAN EFD* bare hull w/o BK	IIHR CFD bare hull w/o BK	Present CFD bare hull w/o BK
0.20	4.54N	-18.6%	-15.7%	-17.9%

*EFD results are from Cook (2011)

Self-propulsion Simulation

For self-propulsion simulation, the ONR Tumblehome ship model is equipped with twin rotating propellers and twin controller rudders. It is one of the benchmark cases (case 3.9) in Tokyo 2015 CFD Workshop in ship hydrodynamics. According to the case setup, the fully appended ship is set to free running at model point in calm water. The approaching speed is $U_0 = 1.11$ m/s ($Fr = 0.20$), and target yaw angle is $\psi_C = 0$. The two rotating propellers provide the thrust for the ship to move forward and the controller rudders are performed to maintain the ship moving straight forward. The rotating propellers are controlled by the PI controller and moving rudders are performed by the P controller as shown in Equation (4) and Equation (7) respectively. Overset grid arrangement and mesh distribution is described in Figure 2-4, and the size of each part grid is shown in Table 2.

To accelerate the convergence of the calculation, the initial state of the self-propulsion simulation is obtained by interpolating data from the final flow field of the towed condition, which as a result can save large amount of computational time. This step is conducted by the *mapFields* utility, which is a pre-processing tool in OpenFOAM. During the self-propulsion simulation, the ship model is free to all degrees of freedom with an initial target advancing velocity U_0=1.11m/s .The twin propellers start from static state and speed up the rotational velocity to provide enough thrust. The proportional and integral coefficients *P* and *I* are set to 800 and the detailed process of the PI controller is described in the numerical approach part.

The time histories of the rate of resolutions (RPS) of propellers and ship model advancing speed are shown in Figure 10. From the figure we can see that the RPS starts from zero and increases quickly. The curves of the RPS converge to the desired the value in about 5s. According to the numerical results, the ship speed decreases at first due to less thrust provided by the rotational propellers and as the RPS of propellers increases, the increasing thrust can let the ship speed come back to the target value. Figure 9 also presents the comparison between the numerical results and experimental results for time histories of RPS. The predicted RPS shows overall agreement with the experiment, which indicates our present approach for self-propulsion simulation is applicable.

Predicted force coefficients are made non-dimensional with the wetted surface area at rest S_0, fluid density ρ and ship advancing speed U. Force coefficients are defined as follows:

$$C_T = \frac{R_T}{\frac{1}{2}\rho U^2 S_0} \tag{12}$$

$$C_F = \frac{R_F}{\frac{1}{2}\rho U^2 S_0} \tag{13}$$

$$C_P = \frac{R_P}{\frac{1}{2}\rho U^2 S_0} \tag{14}$$

Table 4 lists the numerical results of ship motions and self-propulsion coefficients.

Table 4 Ship motions and self-propulsion coefficients

Parameters	EFD	CFD	Error
sinkage $\sigma \times 10^2$ (m)	2.26E-1	2.41E-1	6.5%
trim τ(deg)	3.86E-2	4.64E-2	20.3%
$C_T \times 10^3$		5.291	
$C_F \times 10^3$		3.752	
$C_P \times 10^3$		1.539	
n(RPS)	8.97	8.819	-1.7%
K_T		0.242	
K_Q		0.0746	

From Table 4 we can see that the computational result of sinkage is 6.5% larger than the experimental data while the predicted trim is overestimated by 20.3%. The large percentage error is due to the very small reference value. As with the motions of other degrees of freedom, the amplitude is very small from our simulated results (shown in Figure 11), especially for the yaw motion, which indicates that there is no need to move the rudders

during the simulated time to meet its coursekeeping demand.

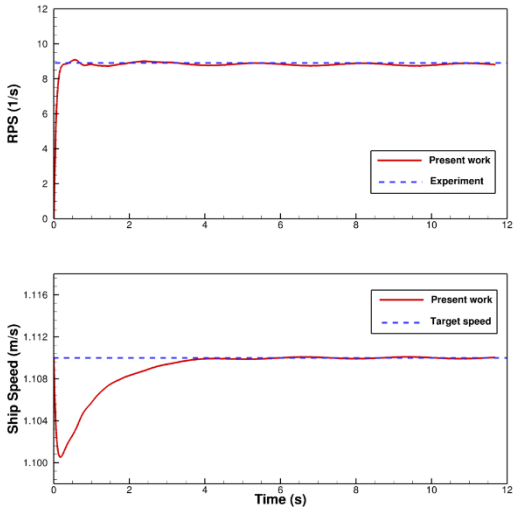

Figure 10 Time histories of RPS and ship speed

Table 4 also shows the propulsive coefficients of the self-propulsion simulation. Since the computation is carried out to predict the self-propulsion model point, none of the coefficients except *n* can be compared with the measured data. The rate of revolutions of the propeller *n* computed by our own solver naoe-FOAM-SJTU is 8.819, which is underestimated by about 1.7% than that of the experimental data. The high accuracy of the predicted rate of resolution of propeller indicates that the present approach can be an alternative way to predict the model point for free running ship model.

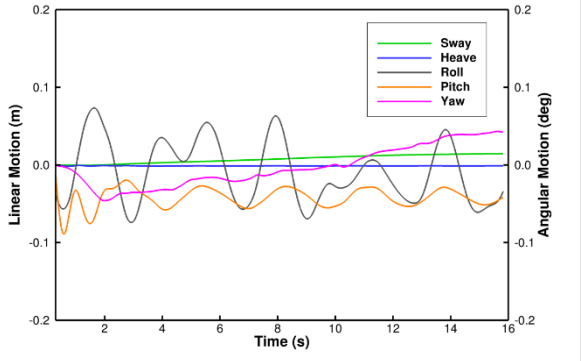

Figure 11 Time histories of ship motions

Figure 12 shows a profile view of vortical structures displayed as isosurfaces of Q=200 colored by axial velocity. From the stern view of the vortical structure, the propeller tip vortices are clearly resolved even around rudders, but dissipate quickly within the coarser mesh downstream. The strong hub vortex observed has a much larger size so that it is still somewhat resolved by the coarser grid downstream of the refinement. From the figure we can also see the vortices after the rudder root, which is caused by the gap between the rudder and rudder root, and this will not come out in the real test.

Figure 13 shows a 3D view of the vortical structure, where strong interaction between the propeller vortex and the rudder geometry exists. The strong hub vortex of the propeller is not affected by the rudder. This is due to the fact that the axis of the rudder is not aligned with the axis of propeller. An interesting phenomenon occurs when the tip vortices of blades pass through the rudders, where the vortices separated rapidly at the top side. The strong flow interaction between the propellers and rudders can result in complex hydrodynamic performance of ship hull, especially when the rudders are in prescribed maneuver mode.

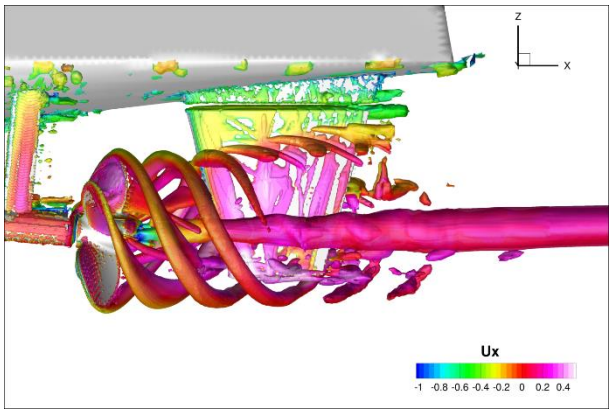

Figure 12 Profile view of Q contour

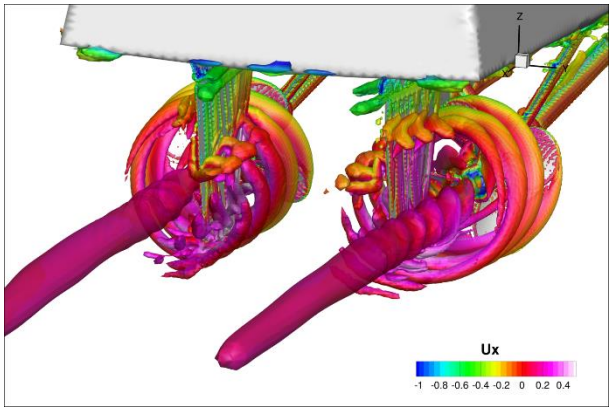

Figure 13 3D view of Q contour

SIMULATION PART II: TURNING CIRCLE

The assessment of turning maneuvering characteristics such as advance, transfer, and tactical diameter are important for ship safety when maneuvering in or out of harbors and turning is required (IMO, 2002). The definition of these parameters is shown in Figure 14.

Standard turning circle test with 35° rudder angles were carried out for the present numerical simulation. During the procedure, the rate of resolution RPS is set to 8.819 according to the self-propulsion result and the calculation is restarted from the steady state of the self-propulsion. At first, the rudder is static for the ship model to move forward for about 1s at model scale time and after that the rudders start to execute at rudder rate 35°/s. The rudders turn to the target value in 1 second and the ship model moves freely according to the forces excited by moving rudders. Due to the large amount of computational time with full discretized hull, propeller, and rudder model, the calculation is executed only in one turning period, which in other words, the pull-out angle is set to 360°.

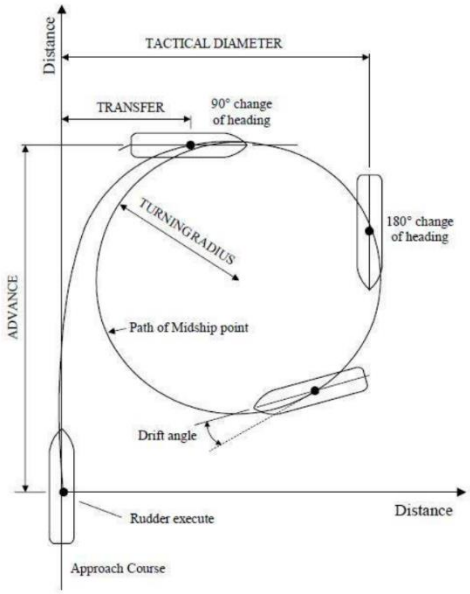

Figure 14 Definition of turning parameters (from ABS maneuvering guide, 2006)

Simulation Results

In Figure 15 the trajectory of the turning circle simulation is presented and compared with the experimental result by Elshiekh (2014).

The comparison in terms of the turning circle trajectory shows an overall agreement between the numerical result and the experimental data (Figure 15). Conversely, the numerical results predict a larger turning diameter compared with the experiment. Table 5 lists the comparison of turning circle parameters, i.e. advance, transfer, tactical diameter, and turning diameter. From the table we can see that the numerical simulation can give a good prediction of the maneuvering characteristics.

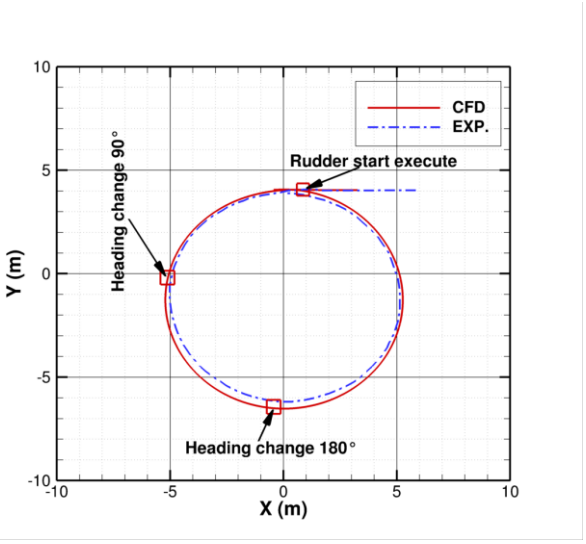

Figure 15 Trajectory of turning circle simulation

Table 5 Comparison of trajectory parameters

Parameters		CFD	EFD	Error
Advance (m)	A_D	7.2854	7.4806	-2.61%
Transfer (m)	T_R	4.3255	4.0539	6.69%
T_{90} (s)		15.9872	15.1400	5.59%
Tactical (m)	T_A	10.4581	10.0068	4.51%
T_{180} (s)		27.5894	26.0700	5.83%
Turning (m)	T_D	10.5431	10.1481	3.89%

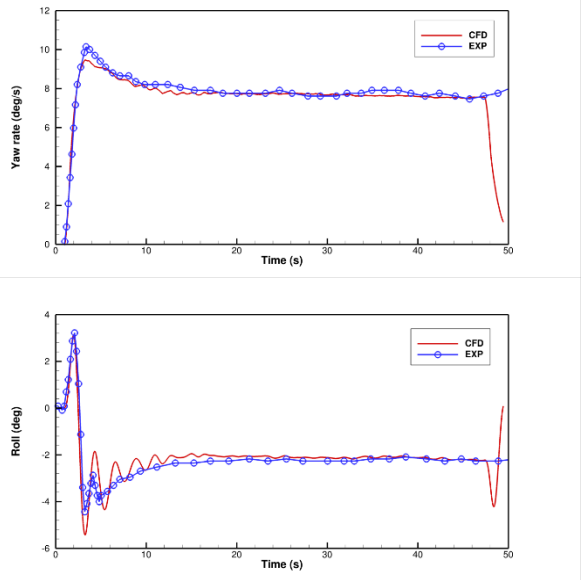

Figure 16 Time histories of yaw rate and roll motion

The time histories of yaw rate and roll motion of ship hull in one turning period are shown in Figure 16.

Immediately after the execution of the rudder, the ship model achieves an increasing positive yaw rate, and the yaw rate experience its peak value after the rudder complete its rotation.

A similar behavior is experienced in the time histories of the roll motion. But discrepancy shows up with two peaks for the roll motion, where the ship model first turn to its port side with the peak value of about 3.13° and then it turns to its starboard side with the peak value of 5.42°. After the first stage of transient phase in roll motion, it gradually comes to a stabilized value of 2.08°. The differences at the end of the curves shown in both comparison of yaw rate and the roll motion is due to the pull out phenomena for the CFD simulation while the experiment will go several other rounds. Other than this, the simulation shows overall agreement with the experimental result, whereas the peak values for both yaw rate and roll motion is underestimated to some extent.

Transient Phase Analysis

The transient phase during the rotation of the rudders plays an important role in the hydrodynamic performance of ship hull. To properly estimate the effect of rudder deflection, several snapshots of the flow field around twin propellers and rudders are presented to illustrate the characteristics in the first transient phase. Figure 17 shows the detailed vorticity field around twin propellers and rudders, where 6 snapshots with different instant rudder angles (θ) are presented. The flow field is colored by vorticity magnitude at horizontal sections around twin propellers and rudders.

The vorticity field is almost symmetry at the first static phase and soon after the execution of rudders, the vorticity field then gradually becomes very complex. As the rudders are actuated to the starboard side, the hub vortex of the windward propeller is barely affected by the rudder behind it. However, the hub vortex of the leeward propeller is strongly affected by the rudder since the rudder block the way of the hub vortex advancing. Furthermore, it can be seen from the figure that the vortex of the skeg can also produce consequences for the leeward propeller and rudder. Due to the highly asymmetry flow field of the twin propellers and rudders, the hydrodynamic forces especially the lateral forces of rudders are significantly different. Figure 18 presents the time histories of lateral forces of the twin rudders. At the static phase, the lateral forces of the leeward and windward rudder is asymmetry and the total lateral force acted on the ship hull is zero (no turning forces). As the rudder is executed at $t = 1s$, the lateral forces show different changes for the leeward rudder and windward rudder, where the leeward rudder increases all the way up and the windward rudder first decreases and then increases to a certain value with the same direction of leeward rudder. As a result, the total lateral force on the ship hull increases and the model is then under turning circle phase.

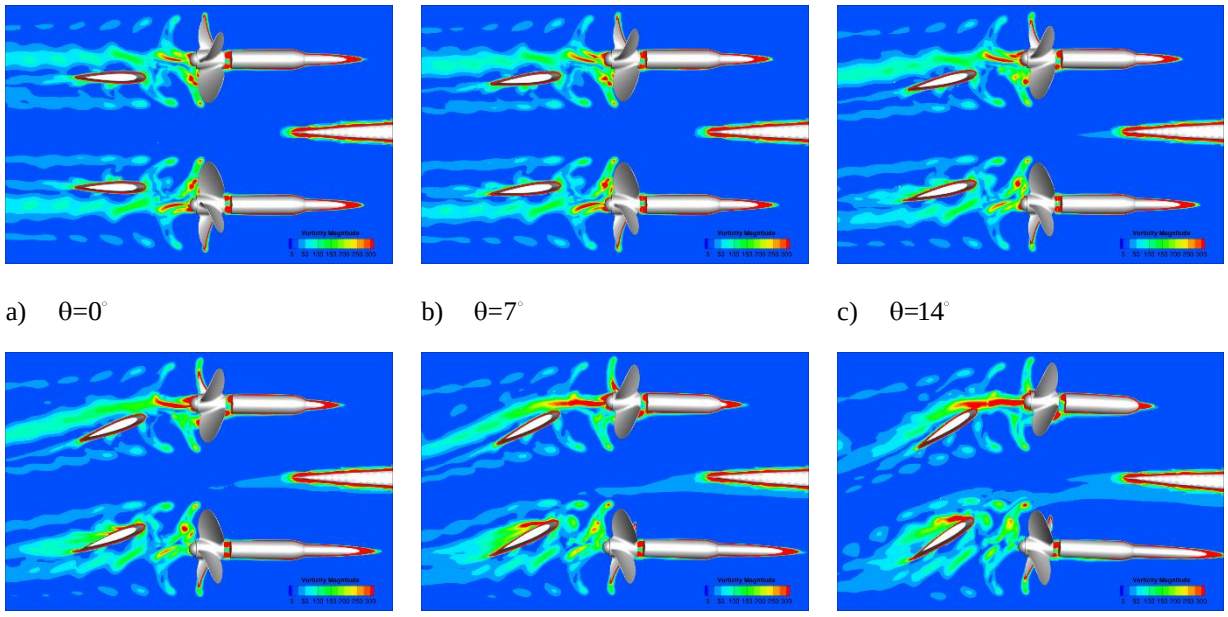

a) $\theta=0^{\circ}$ b) $\theta=7^{\circ}$ c) $\theta=14^{\circ}$

d) $\theta=21^{\circ}$ e) $\theta=28^{\circ}$ f) $\theta=35^{\circ}$

Figure 17 Vorticity field around twin propellers and rudders at horizontal sections

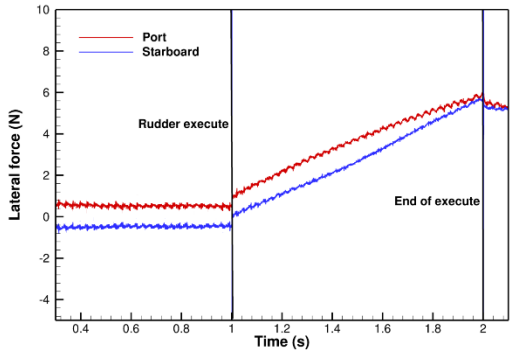

Figure 18 Time histories of lateral forces of the leeward and windward rudder

Stabilized Phase Analysis

After the first transient phase, the ship model undergoes the turning circle phase, which is also called the stabilized phase. During this stage, the main contribution to the ship is a stabilizing yaw moment exerted by the twin propellers and rudders. In fact, the leeward propeller provides a very small lateral force while the windward propeller makes a large contribution to the lateral force.

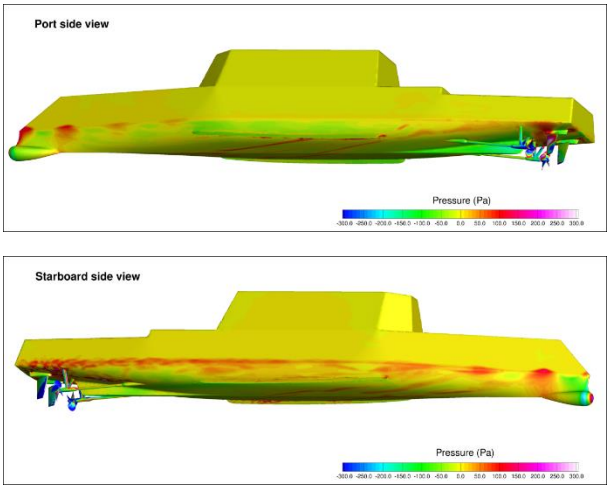

Figure 19 Pressure distribution on the ship hull, propellers, and rudders during the steady phase of the turn.

In order to gain more insight into the hydrodynamic characteristics of the stabilized phase, a zoomed view of pressure distribution on ship hull, propellers and rudders were depicted in Figure 19.

It can be seen from the pressure distribution that the starboard side experienced higher pressure on the ship hull than that of the port side during the stabilized phase. From the view of bow, the leeward pressure is lower than the windward, which leads to a turning moment. From the view of stern, the pressure in the leeward side is higher than that of windward side, which also provides a same turning moment for the ship hull. Another phenomenon we can observe is that there are several sudden changes at the bottom of the ship hull, which is due to the vortical structures shown in Figure 20.

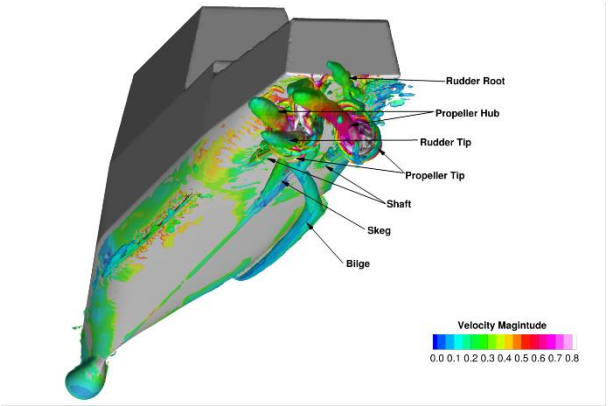

Figure 20 Vortical structure around fully appended ship hull, twin propellers and rudders during the stabilized phase.

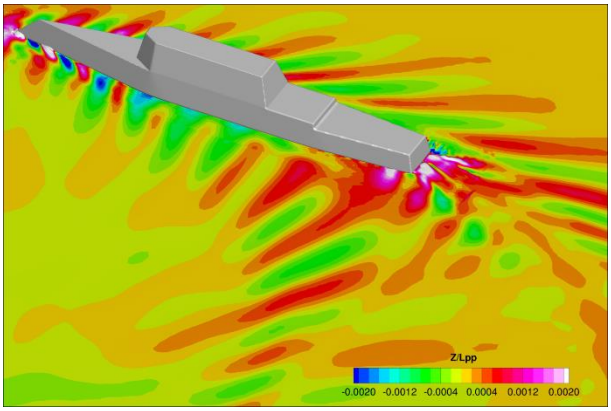

Figure 21 Wave pattern in stabilized phase during turning circle simulation.

Figure 20 shows a global view of vortical structure displayed as isosurfaces of Q=200 colored by velocity magnitude. Compared to the self-propulsion simulation, the vortical structure in turning circle is of higher complexity with strong interaction between appendages, propellers and rudders. The vortex of the bilge is observed in the starboard side and it strongly affects the vortex of leeward propeller and the skeg. This is how the sudden change of pressure distribution in the bottom of ship hull mentioned above comes out. In this figure, the propeller tip vortices are clearly resolved and dissipate quickly within the coarser mesh downstream. The hub vortex observed has a change with its path compared to

self-propulsion simulation. Another effect occurs when the hub vortex of leeward propeller passes through the leeward rudder, where the vortex becomes highly nonlinear due to the rudder deflection.

Free surface during the stabilized phase is depicted in Figure 21 colored by the wave height. The wave pattern is different from that of the towed condition, where the stern wave show highly asymmetry due to the turning of the ship. As the consequence of stabilized phase, the port side bow wave is also bigger than the starboard side.

GRID CONVERGENCE STUDY

With the fact of the large amount of computational time required by the self-propulsion and turning circle simulation, grid convergence study is only conducted on the open water calculation in the present work. On the other hand, the simplicity of the overset grid arrangement in open water calculation (only two part of grid is applied) makes it suitable for the convergence study. Three grids with a refinement ratio of $\sqrt{2}$ in each direction are carried out for the convergence study. Considering the grids used in the present calculation is fully unstructured, the systematic refinement in three directions is very difficult to handle. In order to do the grid refinement, an alternative approach is applied as follows. The background Cartesian grid required by the *snappyHexMesh* is refined by splitting cells. Three systematic background grids with specified refinement ratio are taken into account. The final generated grids are approximately refined according to the grid convergence study.

Grid convergence study in the present work follows the recommended procedures and guidelines (ITTC, 2008). Result changes between medium-fine $\varepsilon_{21}=S_2-S_1$ and coarse-medium $\varepsilon_{32}=S_3-S_2$ are used to define the convergence ratio:

$$R_G = \frac{\varepsilon_{21}}{\varepsilon_{32}} \tag{15}$$

and to determine convergence condition, where S_1 S_2 and S_3 correspond to solutions with fine, medium, and coarse grid, respectively. Three convergence conditions are possible:

$$\begin{aligned} &\text{(I)} \quad \text{Monotonic convergence}: 0 < R_G < 1 \\ &\text{(II)} \quad \text{Oscillatory convergence}: R_G < 0 \\ &\text{(III)} \quad \text{Divergence}: R_G > 1 \end{aligned} \tag{16}$$

For condition (*III*), grid convergence study cannot be estimated.

The grid convergence study is carried out at $J=1.0$ for the open water case with respect to the most approximate condition to the propeller at self-propulsion and turning circle simulation. Hydrodynamic parameters K_T , K_Q and η_0 are used to estimate the grid convergence. Table summarizes the results of the grid convergence study.

Table 6 Results of grid convergence study at J=1.0

Grid	ID	Grid Size	K_T	Error (%)	K_Q	Error (%)	η_0	Error (%)
EFD			0.2638		0.0734		0.5723	
Fine	S_1	3.892M	0.2635	-0.113	0.0763	3.951	0.5496	-3.966
Medium	S_2	1.233M	0.2632	-0.226	0.0782	6.539	0.5357	-6.395
Coarse	S_3	0.576M	0.2594	1.668	0.0806	9.809	0.5122	-10.501
R_G			0.0789		0.7916		0.5915	
Convergence			Monotonic		Monotonic		Monotonic	

It can be seen from
Table **6** that the thrust coefficient K_T shows monotonic convergence with R_G=0.078 and the predicted value of K_T is highly accurate with errors under 1.7%. The torque coefficient K_Q is overestimated by all three grids with errors up to 9.8% and the efficiency η_0 is underestimated with largest error of -10.5%. Both torque coefficient and efficiency show monotonic convergence with $R_G = 0.7916$ and 0.5915, respectively.

Note that the grid size of the self-propulsion and turning circle simulation is larger than medium grid but smaller than the fine grid. This indicates that the propeller grid used in the free maneuvering simulation will slightly change the numerical results.

CONCLUSIONS

This paper presents the free maneuvering simulations of fully appended ONR Tumblehome. Two situations, i.e. 6DoF self-propulsion and turning circle simulation, are carried out using self-developed CFD solver naoe-FOAM-SJTU. During the process, the moving rudders and rotating propellers are handled by the dynamic overset grid method. For the 6DoF self-propulsion simulation, a proportional-integral (PI) controller is employed to adjust the rotational rate of the propeller to achieve the desired ship speed and a P controller is applied to maintain its heading. For the turning circle simulation, a specified maneuver rudder is used to achieve the desired turning motion.

Open water calculations were carried out using the single-run method and the numerical results show an overall agreement with the experiment performed at IIHR. Furthermore, the grid convergence study is also applied in this situation and the predicted coefficients, i.e. K_T, K_Q and η_0 , show monotonic convergence. Towed condition for bare hull model is carried out to give an approximate initial state of the self-propulsion computation to reduce time consumption. Predicted rate of resolution (RPS) of propellers at self-propulsion simulation is 1.7% lower than that of the experiment, which indicates that the present approach is applicable for the free running simulation. Detailed information of the flow field around twin propellers and rudders are depicted and analyzed to explain the strong interaction of the ship hull, propellers and rudders. Ship motions except advancing in self-propulsion simulation are very small and there is no need to do the rudder control. Turning circle simulation is started from the final state of the self-propulsion, and the rotational speed of twin propellers are fixed to the predicted value of $n = 8.819$. The numerical results of turning circle trajectory and time histories of yaw rate and roll motion are presented and compared to the experiment. Good agreement is observed for the turning diameter with error of 3.89%. Other turning parameters are also in accordance with the experimental data. Furthermore, the transient phase and stabilized phase are analyzed in detail through the corresponding flow field. Vorticity field at the horizontal section during the rudder execution is presented to illustrate the transient phase character. Strong interaction between vortices of bilge, skeg and twin rudders and propellers are observed in stabilized phase.

Future work will focus on the full 6DoF self-propulsion simulation in waves especially in oblique waves to investigate the rudder maneuver behavior in coursekeeping simulation. More work will be done to do the verification and validation of the fully appended ship hull, propeller and rudder computation.

ACKNOWLEDGEMENTS

This work is supported by the National Natural Science Foundation of China (51379125, 51490675, 11432009, 51579145, 11272120), Chang Jiang Scholars Program (T2014099), Program for Professor of Special Appointment (Eastern Scholar) at Shanghai Institutions of Higher Learning (2013022), and Innovative Special Project of Numerical Tank of Ministry of Industry and Information Technology of China (2016-23/09), to which the authors are most grateful.

REFERENCES

American Bureau of Shipping, "Guide for Vessel Maneuverability," Houston, TX, 2006.

Broglia, R., Dubbioso, G., Durante, D. and Mascio, D. A., "Turning Ability Analysis of a Fully Appended Twin Screw Vessel by CFD," Ocean Engineering, Vol. 105, July, 2015, pp. 275-286.

Cao, H. and Wan, D. C., "Development of Multi-directional Nonlinear Numerical Wave Tank by naoe-FOAM-SJTU Solver", International Journal of Ocean System Engineering, Vol. 4, No. 1, 2014, pp. 52-59.

Cao, H. and Wan, D. C., "RANS-VOF Solver for Solitary Wave Run-up on a Circular Cylinder," China Ocean Engineering, Vol. 29, No. 2, 2015, pp. 183-196.

Carrica, P. M., Ismail, F., Hyman, M., Bhushan, S. and Stern, F., "Turn and Zigzag Maneuvers of a Surface Combatant using a URANS Approach with Dynamic Overset Grids," Journal of Marine Science and Technology, Vol. 18, No. 2, Sept. 2012, pp. 166-181.

Carrica, P. M., Mofidi, A. Eloot, K. and Delefortrie, G., "Direct Simulation and Experimental Study of Zigzag Maneuver of KCS in Shallow Water," Ocean Engineering, Vol. 112, 2016, pp. 117-133.

Cook, S.S., "Effects of headwinds on towing tank resistance and PMM tests for ONR Tumblehome," Master Thesis, THE UNIVERSITY OF IOWA, 2011.

Elshiekh, H., "Maneuvering Characteristics in Calm Water and Regular Waves for ONR Tumblehome," Master Thesis, THE UNIVERSITY OF IOWA, 2014.

Ferziger, J. H. and Peric, M., "Computational Methods for Fluid Dynamics," Springer Science & Business Media, 3rd rev. ed., 2012.

Issa, R. I., "Solution of the Implicitly Discretised Fluid Flow Equations by Operator-splitting," Journal of Computational Physics, Vol. 62, No. 1, Jan. 1986, pp. 40–65.

International Marine Organization, "Standards for Ship Maneuverability," MSC. Vol. 137, No.76, 2002.

ITTC, "CFD, Resistance and Flow Uncertainty Analysis in CFD Examples for Resistance and Flow," ITTC-

Recommended Procedures and Guidelines, 7.5-03-02-01, 2008, pp. 1-12.

Menter, F. R., "Review of the Shear-stress Transport Turbulence Model Experience from an Industrial Perspective," International Journal of Computational Fluid Dynamics, Vol 23, No.4, Apr. 2009, pp. 305-316.

Noack, R. W., Boger, D. A., Kunz, R. F. and Carrica, P. M., "Suggar++: An Improved General Overset Grid Assembly Capability," Proceedings of the 19th AIAA Computational Fluid Dynamics Conference, San Antonio TX, USA, June, 2009, pp. 22-25.

Sanada, Y., Tanimoto, K., Takagi, K., Gui, L., Toda, Y. and Stern, F., "Trajectories for ONR Tumblehome Maneuvering in Calm Water and Waves," Ocean Engineering, Vol. 72, Nov. 2013, pp. 45-65.

Shen, Z. and Wan, D. C., "An Irregular Wave Generating Approach Based on naoe-FOAM-SJTU Solver," China Ocean Engineering, Vol. 30, No. 2, 2015, pp. 177-192.

Shen, Z., Wan, D. C. and Carrica, P. M., "Dynamic Overset Grids in OpenFOAM with Application to KCS Self-propulsion and Maneuvering," Ocean Engineering, Vol. 108, Nov. 2015, pp. 287-306.

Shen, Z. and Wan, D. C., "Manual of CFD solver for ship and ocean engineering flows: naoe-FOAM-SJTU," Technical Report for Solver Manual, Shanghai Jiao Tong University, 2014.

Van Leer, B., "Towards the Ultimate Conservative Difference Scheme. V. A Second-order Sequel to Godunov's Method," Journal of Computational Physics, Vol. 32, No. 1, July, 1979, pp. 101-136.

Wang, J., Liu, X. and Wan, D. C., "Numerical Simulation of an Oblique Towed Ship by naoe-FOAM-SJTU Solver," Proceedings of the 25th International Offshore and Polar Engineering Conference, Big Island, Hawaii, USA, 2015, pp.432-438.

Wang, J., Liu, X. and Wan, D. C., "Numerical Prediction of Free Running at Model Point for ONR Tumblehome using Overset Grid Method," Proceedings of Tokyo 2015 Workshop on CFD in Ship Hydrodynamics, Vol. III, Dec. 2-4, 2015, NMRI, Tokyo, Japan, pp. 383-388

Xing, T., Carrica, P. M. and Stern, F., "Computational Towing Tank Procedures for Single Run Curves of Resistance and Propulsion", Journal of Fluids Engineering, Vol. 130, No. 10, Sept. 2008, 101102.

DISCUSSION

Takanori Hino

Yokohama National University

Questions for discussion are as follows:

1. In Figure 8, there seem to be the reflected waves on the side of the hull. Did the authors apply special treatment to the outlet boundary to suppress wave reflections?
2. In Figure 10, although very small, the yaw motion is observed and the sway shows drift motion. Since the geometry is symmetric, the flow field must be also symmetric and the rudder control is not activated. What is the reason why the ship motion is not symmetric?
3. The grid convergence study for the propeller open water simulation adopted the successively refined grids. Though the authors described the parameters for the background Cartesian grids, the information is not given for the boundary layer grids near the wall. How the minimum spacing, the number of the layers and the stretching ratio are controlled for the series of the grids?

AUTHOR'S REPLY

Thank you for your questions and comments, here are the responds:

Question 1: First I want to explain that Figure 8 is just a local view of the wave pattern and the computational domain extends to $-1.5Lpp < x < 5.0Lpp$, $-1.5Lpp < y < 1.5Lpp$, $-1.0Lpp < z < 0.5Lpp$. The side of the computational domain applies the farfield boundary condition, where zero velocity and zero gradient of pressure is imposed. And for outlet boundary, we applied a special velocity boundary condition called the *outletPhaseMeanVelocity*, which is a built-in scheme in OpenFOAM and this boundary condition adjust the velocity for the given phase to achieve the specified mean thus causing the phase-fraction to adjust according to the mass flow rate. It's a typical boundary for the outlet condition of the towing-tank ship simulation to maintain the outlet water level at the level as the inlet.

A new figure as well as the illustration for the boundaries are added in the manuscript to explain this.

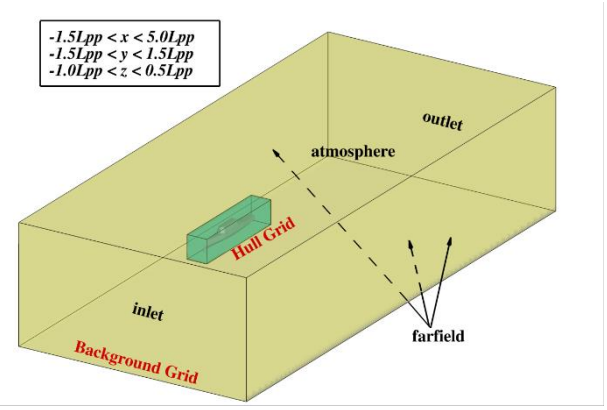

Figure 1 Computational domain for towing condition

Question 2: In my opinion, the reason for the asymmetry is as follows:

1) The generation of the mesh is through the OpenFOAM utility *snappyHexMesh*, and the 3-dimensional meshes are automatically generated from the triangulated surface geometries. The mesh approximately conforms to the surface by iteratively refining a starting mesh and morphing the resulting split-hex mesh to the surface. As a result, the grid around the fully appended ship hull can be slightly asymmetric after the iteration process.
2) The initial flow state is mapped from the final state of towed condition, and the map process can result in little difference with the flow information for both side around ship hull.
3) For the full viscous flow calculation, the separation of the vortices from the fully appended ship model is an unsteady problem and can lead to the asymmetry of the flow field.
4) Another reason may be the numerical error during the calculation.

For the ideal situation, the flow field must be symmetric, but when all the degrees of freedom are free, slight disturbance can result in the asymmetry of the simulation result.

Question 3: As described in the manuscript, the grid is refined through splitting cells from the initial background

Cartesian grid. During the mesh generation, the boundary layer mesh is controlled by a subDict of the *snappyHexMesh* called the *addLayersControls*. Four main parameters are used in the boundary layer control, namely, relative size, number of layers, expansion ratio and final layer thickness. The relative size specifies the boundary layer size is relative to the undistorted cell size outside layer. That is to say, when we generate the boundary layer mesh, the mesh size of the boundary layer is according to the size of the first level cell outside the ship hull. As for the grid convergence study, the control parameters for the boundary layer is the same, and in this way, the final layer mesh size can be relative to the refinement ratio of the three grids. In the present work, the number of the boundary layer is 4 and the expansion ratio is 1.2.